Hybrid Simulation-Measurement Calibration Technique for Microwave Imaging Systems

Hybrid Simulation-Measurement Calibration Technique for Microwave Imaging Systems

D. O. Rodriguez-Duarte, J. A. Tobon Vasquez, F. Vipiana
Dept. Electronics and Telecommunications, Politecnico di Torino, Torino, Italy,
{david.rodriguez, jorge.tobon, francesca.vipina}@polito.it

***Abstract*—This paper proposes an innovative technique to calibrate microwave imaging (MWI) systems combining available measured data with simulated synthetic ones. The introduced technique aims to compensate the variations of the antenna array due to unavoidable manufacturing tolerances and placement, in comparison to the nominal electromagnetic (EM) scenario. The scheme is tested virtually and experimentally for the MWI of the adult human head tissues. The virtual EM analysis uses a realistic 3-D CAD model working together with a full-wave software, based on the finite element method. Meanwhile, the real implementation employs a single-cavity anthropomorphic head phantom and a custom brick-shaped antenna array working at around 1 GHz.**

***Index Terms*—Measurements calibration, microwave imaging, numerical simulation, microwave antenna arrays, microwave propagation.**

I. Introduction

Microwave imaging (MWI) is an upcoming technology that has emerged as a promising alternative in several fields due to its attractive features of penetration, sensitivity to dielectric contrast, non-invasiveness, harmlessness, and cost-effectiveness [1], [2]. The considered inverse scattering problems are non-linear and ill-posed, and employ mapping domains that cannot be assessed directly or are extremely difficult to reach [1]. For instance, in medical imaging-based diagnosis, it is being applied to recover images of pathologies such as breast cancer and brain stroke [3]–[11]. Moreover, in food contamination detection is used to localize small plastic contaminants within food container [12], and in grain-storage for detect spoiled zones [13].

The principle of MWI relies on the contrast of the electrical properties (permittivity and conductivity) that present the different regions of the imaging domain(DOI) at microwave frequencies, e.g., in the brain stroke diagnosis, the contrast is between healthy tissues of the brain and the stroke-affected area. Generally, an MWI system consists of an array of identical antennas around the DOI acting as transmitters and receivers. The antennas then sample the total and incident fields, from which the imaging algorithm recovers the scattered field in the DOI. The algorithm applies either direct procedures such as the distorted Born approximation –applicable in the case of weak scatters– and truncated singular value decomposition (TSVD) [14], or iterative ones such as the distorted Born iterative method (DBIM) or the contrast source inversion (CSI) algorithm [15], [16].

The inversion mechanisms (i.e., the whole imaging algorithm) employs at least once the solution of the forward problem, which describes the system's electromagnetic (EM) behavior. It is an essential element to reach outcomes with adequate accuracy, reliability, and quality. Thus, accurate and realistic numerical modeling provides faithful EM fields of the scenario under test and allows assessing variations of it without actual implementation. However, it is well-known the real scenarios presents unavoidable tolerances in manufacturing and placements, even using detailed modeling. These issues generate unwanted and non-modeled variations on the operator (e.g., in a real system with multiples antennas, these could have several variations).

Here, we introduce a hybrid simulation-measurement (HS-M) procedure to calibrate the simulated S-parameters, initially computed during the forward problem solution, to the measured ones via a custom set of basis functions obtained from multiple high-fidelity simulations. Thus, the intended scheme attempts to improve each antenna's projected response in an MWI system with real measured data. In this work, we inspired from [17], where the antenna's far-field is recovered from an under-sampled near field via insertion of a-priori information (geometry and materials of the antenna under test) using advanced numerical modeling.

The paper is organized as follows. Section II covers the fundamentals and the mathematical framework of the proposed algorithm. Then, Section III details the scheme to build the used basis functions, and the preliminary results, in either simulation and measured cases, are presented in Section IV. Finally, Sect. V summarizes the conclusions and future work.

II. HS-M Calibration procedure

The proposed HS-M calibration systematically combines a-priori information on the MWI system (i.e., antennas, distribution of the antennas, materials), high-fidelity EM simulations of possible variations of the scenario under test, and measurements at the antenna ports in order to enhance the forecasted system behavior.

A. Basis definition

The procedure starts by expressing the measured S-parameters as a finite linear combination of known basis functions, Ψ_k, with unknown coefficients, α_k,

$$S(\mathbf{r}_m, \mathbf{r}_1, f_i) \cong \sum_{k=1}^{K} \alpha_k \Psi_k(\mathbf{r}_m, \mathbf{r}_1, f_i) \tag{1}$$

for $m = 1, \ldots, N$, where N is the number of antennas, and for $i = 1, \ldots, N_f$, where N_f is the number of measured frequency points; $\mathbf{r}_1$ is the position of the transmitting antenna and $\mathbf{r}_m$ of the receiving ones. Then, the latter can be expressed in matrix format as

$$[S] \cong [\Psi][\alpha], \tag{2}$$

where $[S]$ is an array with length (NN_f) that collects all the measured S-parameters when the antenna 1 is the transmitter, $[\alpha]$ is an array with length K collecting the unknown coefficients α_k, and

$$[\Psi] = [[\Psi_1], \cdots, [\Psi_K]], \tag{3}$$

has dimension $(NN_f) \times K$ and collects all the basis functions $[\Psi_k]$.

The basis functions $[\Psi_k]$ are obtained applying the singular value decomposition (SVD) to K sets of simulated scattering parameters where each simulation of the considered scenario is slightly changed (e.g., changing the transmitter position and geometry). The SVD procedure is applied to extract the minimal number of independent (orthogonal) distributions that maximize information quantity. Hence, $[\Psi]$ corresponds to the left singular vectors of the matrix

$$[S^{\mathrm{sim}}] = \left[[S_1^{\mathrm{sim}}], \cdots, [S_K^{\mathrm{sim}}]\right], \tag{4}$$

where, for each k-th simulation, $[S_k^{\mathrm{sim}}]$ collected the (NN_f) simulated S-parameters when the antenna 1 is the transmitter.

B. Estimation of calibration coefficients

Once the basis $[\Psi]$ has been generared, the coefficient $[\alpha]$ are evaluated as

$$[\alpha] = [\Psi]^{\dagger}[S], \tag{5}$$

where † states for Moore-Penrose pseudo inverse. Moreover, as the basis is derived via the SVD from the simulated S-parameters, it is possible (and convenient to maintain the connection with the known simulated cases) to describe $[\Psi]$ as:

$$[\Psi] = [S^{\mathrm{sim}}][\beta]. \tag{6}$$

Thanks to the orthonormality of the basis [21], the $K \times K$ matrix $[\beta]$ is equal to $[A]^{-1}$, where each element of the matrix $[A]$ corresponds to

$$[A]_{i,j} = \langle [\Psi_i], [S_j]^{\mathrm{sim}} \rangle \tag{7}$$

where $\langle \cdot, \cdot \rangle$ denotes the projection between the two vectors. Hence, substituting (6) in (2) we obtain

$$[S] \cong [S^{\mathrm{sim}}][\beta][\alpha], \tag{8}$$

that can be written also as

$$S(\mathbf{r}_m, \mathbf{r}_1, f_i) \cong \sum_{k=1}^{K} \alpha_k \left[\sum_{h=1}^{K} \beta_{kh} \, S_h^{\mathrm{sim}}(\mathbf{r}_m, \mathbf{r}_1, f_i) \right] \tag{9}$$

Finally, considering that there is a linear relationship between the field radiated by the transmitting antenna and the field on the receiving antenna ports, we can apply this linear operator $\mathcal{L}$ to (9) obtaining

$$\begin{aligned} \mathcal{L}\{S\} &\cong \mathcal{L}\left\{ \sum_{k=1}^{K} \alpha_k \left[\sum_{h=1}^{K} \beta_{kh} \, S_h^{\mathrm{sim}} \right] \right\} \\ &= \sum_{k=1}^{K} \alpha_k \left[\sum_{h=1}^{K} \beta_{kh} \, \mathcal{L}\left\{ S_h^{\mathrm{sim}} \right\} \right] \end{aligned} \tag{10}$$

where $\mathcal{L}\left\{S_h^{\mathrm{sim}}\right\}$ is the simulated radiated field, $\mathbf{E}_h^{\mathrm{sim}}$, for each h-th simulation. Hence, the field radiated by antenna 1 in the region of interest, that is not available by measurements in MWI systems, can be estimated as

$$\widetilde{\mathbf{E}}(\mathbf{r}, \mathbf{r}_1, f) = \sum_{k=1}^{K} \alpha_k \left(\sum_{h=1}^{K} \beta_{kh} \, \mathbf{E}_h^{\mathrm{sim}}(\mathbf{r}, \mathbf{r}_1, f) \right) \tag{11}$$

The described procedure needs to be repeated for all the N transmitters.

III. Applied Model building

In order to preliminary test the HS-M calibration procedure described in Sect. II, we present here a reduced approach using the $S(\mathbf{r}_1, \mathbf{r}_1, f)$ parameter only. Hence, the basis is built via simulations that attempt variations of an MWI realistic scenario. The simulations are obtained with a full-wave advanced numerical model based on an in-house finite element method (FEM) solver working together with a computer-aided design (CAD) software [18].

As MWI 3-D system, we consider the MWI brain stroke imaging prototype recently published in [19]. It consists of a set of 24 brick-shaped antennas employing custom coupling medium [20], which are placed conformally to a human head (i.e., as a helmet). Although all the system antennas are ideally identical, their measured reflection coefficients present variations between them, as shown in Fig. 1(a). Thus, the deviation between antennas is due to the already mentioned manufacturing tolerances and antennas' placements. It was particularly identified that it relies significantly on the slightly different gaps between the antenna's face and the head and the composition of the coupling medium, which varies the permittivity and conductivity of the brick [20]. Then, we construct the basis varying those parametrically.

In the case of gap, the distance [d in Fig. 2 (d)] covers from 0 mm to 10 mm, where 0 mm states for the case when the center of the brick face is touching the head. Meanwhile, the permittivity and conductivity are scaled by a factor between 18.5 and 0.012 S/m, considering reference values 18.5 and 0.012, respectively, as in [20]. Moreover, to render more general the basis, three uniform models of the head are employed, as shown in Figs. 2(a)-(c), where an antenna is placed laterally. The permittivity and conductivity used for the head tissues are an average of the values of the gray and white matter (45.38 and 0.77 S/m at 1GHz) [22].

Fig. 1(b) depicts the reflection coefficients for the different combinations of the gap, permittivity, and head model, and Fig. 3 the singular values (SV) of the considered basis. In the latter, the red segment represents the -85dB truncated SV that is considered during the calibration procedure.

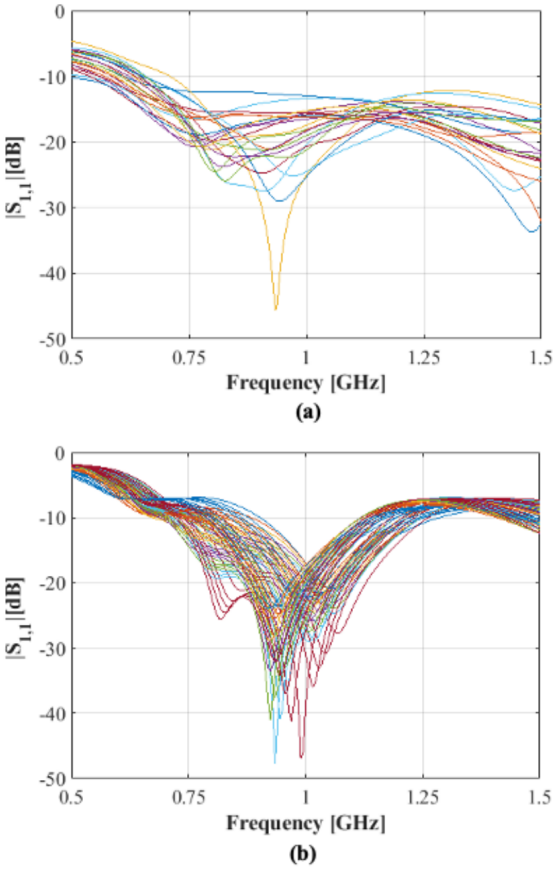

Fig. 1. (a): Measured reflection coefficients of a set of 24 antennas used in [19]; (b): simulated set used for the construction of the basis.

IV. Numerical and Experimental Results

This section presents a preliminary validation of HS-M calibration scheme using both synthetic and measured cases. The first part assesses the capability of the basis to recover the expected $S_{1,1}$ parameter, while the second part considers the use of the scheme for improving the estimation of the field of radiated by one antenna in the region of interest.

Four cases are considered to evaluate the $S_{1,1}$, two using synthetic data and two using actual measured data. In the case of synthetic data, two independent models were built, which are not included in the basis. The first model consists of a brick-shaped antenna filled homogeneously, with a gap $5\,$mm, a 1.05 scaled permittivity and conductivity, and placed on the anthropomorphic head. Instead, the second one consists of a non-homogeneous filled brick (see Fig. 4), where each element of its mesh has a random value of permittivity within a range between 10% with respect to the nominal case. It is placed on the flat model with a gap of $3\,$mm.

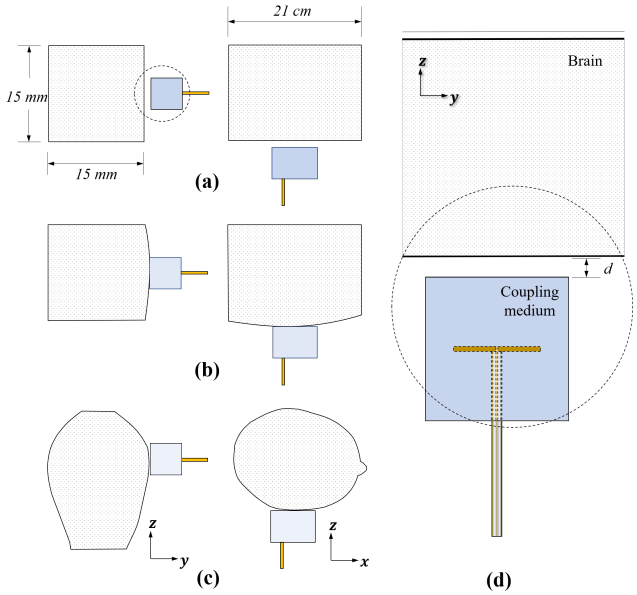

Fig. 2. Models used for generate the basis functions for the correction; (a): flat model where d is the gap distance between antenna and head model; (b): curved model; (c): anthropomorphic head model; (d): Zoom-up view of (a).

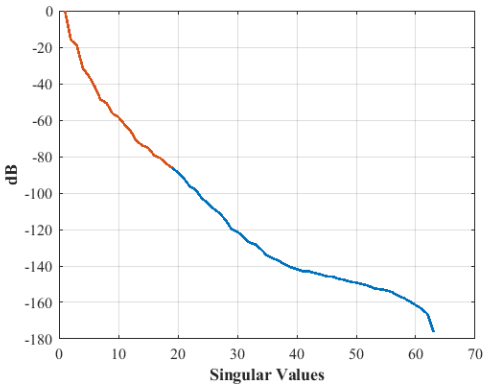

Fig. 3. Singular values of the used basis.

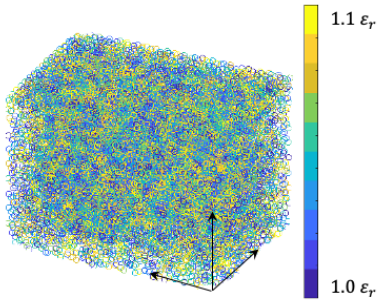

Fig. 4. Non-homogeneous brick antenna. Dimensions as in [20]

Figures. 5 and 6 depict the magnitude and phase of aimed and recovered parameters after applying the calibration scheme for the four studied cases. The results show impressive agreement between target data and the reconstructed ones in simulated and measured cases with an average error lower than 1%. The outcomes confirm the scheme's capability and the built basis to recover synthetic $S_{1,1}$ in different conditions and measured ones.

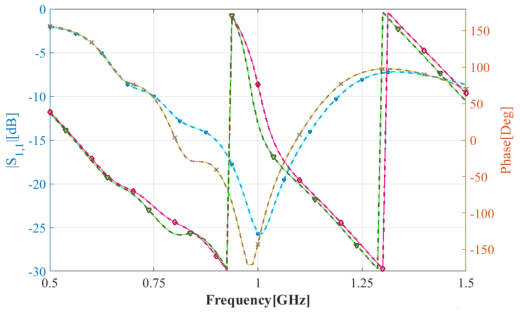

Fig. 5. Reconstruction of S_{11} for two cases using synthetic data (the corresponding reference and reconstructed lines are almost overlapped). Yellow and blue lines refer to the magnitude, and green and pink to the phase.

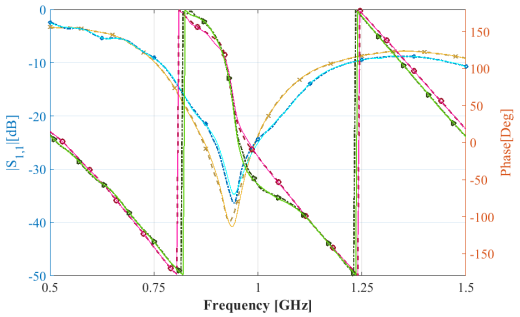

Fig. 6. Reconstruction of S_{11} for two cases using measured data (the corresponding measured and reconstructed lines are almost overlapped). Yellow and blue lines refer to the magnitude, and green and pink to the phase.

As the last test, we presented the reconstructed field radiated by one antenna of the MWI system on a DOI section for the simulated cases at 1 GHz, where the reference field is known. The selected section covers the antenna's frontal area, starting 0.5 cm from the surface of the head model and finishing 14 cm deeper, and encompassing an area of around $7\times14\,\text{cm}^2$. Figure 7 illustrates from top to bottom the target field (synthetic one), the nominal one (expected field without applying the proposed HS-M calibration procedure), and the reconstructed one for the case of homogeneous brick. Instead, Fig.8 considers the case non-homogeneous, where (a) refers to the aimed field and (b) to the calibrated one.

V. Conclusion and Perspectives

This work presented a hybrid calibration technique for microwave imaging systems using both simulated and measured data. It mitigates the effects of unavoidable alterations of the ideal modeled antennas due to the manufacturing process and placement. The technique is preliminarily assessed using a compact version of the scheme. The tested version employs a single antenna. Thus it used the $S_{1,1}$ parameters and showed the potential to reconstruct measured parameters from a synthetically built basis. The next steps further validate the proposed calibration procedure and apply it in the MWI system presented in [19] to improve its imaging capabilities.

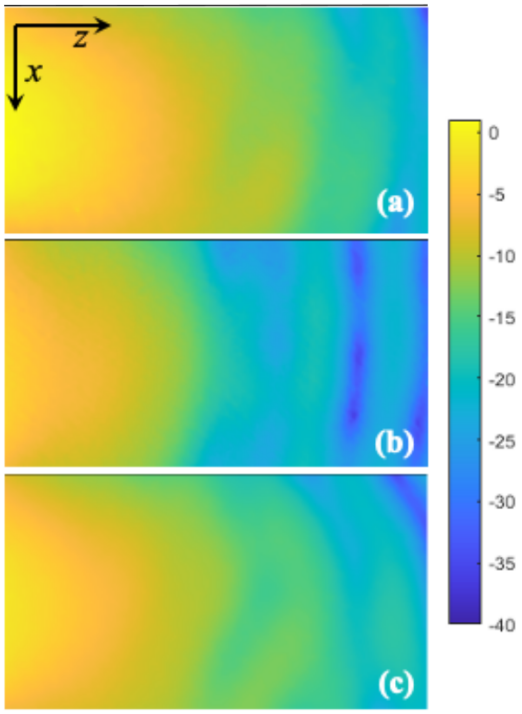

Fig. 7. Recovered electric field radiated by the homogeneous antenna scaled in dBV/m; (a): target field, (b): nominal field, (c): reconstructed field.

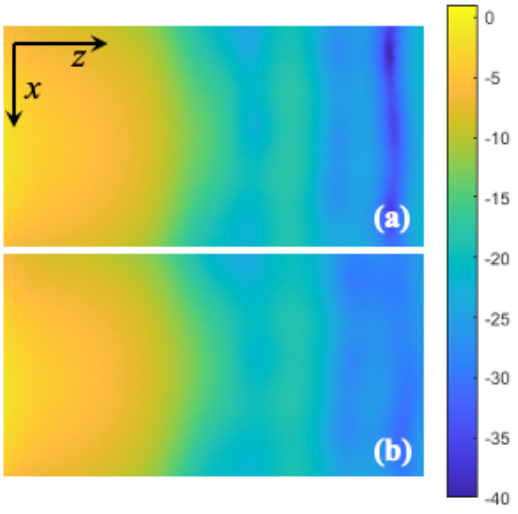

Fig. 8. Recovered electric field radiated by the non-homogeneous antenna scaled in dBV/m; (a): target field, (b): reconstructed field.

ACKNOWLEDGMENT

This work was supported by the Italian Ministry of University and Research under the PRIN project "MiBraScan", and by the European Union's Horizon 2020 Research and Innovation Program under the EMERALD project, Marie Sklodowska-Curie grant agreement No. 764479.

REFERENCES

[1] N. K. Nikolova, Introduction to Microwave Imaging. Cambridge: Cambridge University Press, 2017.

[2] L. Crocco , I. Karanasiou , M. James , R. Conceição (eds), Emerging Electromagnetic Technologies for Brain Diseases Diagnostics, Monitoring and Therapy. Springer, 2018

[3] D. O'Loughlin, M. O'Halloran, B. M. Moloney, M. Glavin, E. Jones and M. A. Elahi, "Microwave Breast Imaging: Clinical Advances and Remaining Challenges," in IEEE Transactions on Biomedical Engineering, vol. 65, no. 11, pp. 2580-2590, Nov. 2018, doi: 10.1109/TBME.2018.2809541.

[4] M. Persson et al., "Microwave-Based Stroke Diagnosis Making Global Prehospital Thrombolytic Treatment Possible," in IEEE Transactions on Biomedical Engineering, vol. 61, no. 11, pp. 2806-2817, Nov. 2014, doi: 10.1109/TBME.2014.2330554.

[5] B. J. Mohammed, A. M. Abbosh, S. Mustafa and D. Ireland, "Microwave System for Head Imaging," in IEEE Transactions on Instrumentation and Measurement, vol. 63, no. 1, pp. 117-123, Jan. 2014, doi: 10.1109/TIM.2013.2277562.

[6] M. R. Casu et al., "A COTS-Based Microwave Imaging System for Breast-Cancer Detection," in IEEE Transactions on Biomedical Circuits and Systems, vol. 11, no. 4, pp. 804-814, Aug. 2017, doi: 10.1109/TBCAS.2017.2703588.

[7] R. Scapaticci, J. Tobon, G. Bellizzi, F. Vipiana and L. Crocco, "Design and Numerical Characterization of a Low-Complexity Microwave Device for Brain Stroke Monitoring," in IEEE Transactions on Antennas and Propagation, vol. 66, no. 12, pp. 7328-7338, Dec. 2018, doi: 10.1109/TAP.2018.2871266.

[8] I. Merunka, A. Massa, D. Vrba, O. Fiser, M. Salucci, and J. Vrba, "Microwave tomography system for methodical testing of human brain stroke detection approaches," *Int. J. Antennas Propag.*, no. Article ID 4074862, 2019.

[9] A. Fedeli, C. Estatico, M. Pastorino, and A. Randazzo, "Microwave detection of brain injuries by means of a hybrid imaging method," *IEEE Open Journal of Antennas and Propagation*, pp. 1–11, 2020.

[10] A. S. M. Alqadami, N. Nguyen-Trong, B. Mohammed, A. E. Stancombe, M. T. Heitzmann, and A. Abbosh, "Compact unidirectional conformal antenna based on flexible high-permittivity custom-made substrate for wearable wideband electromagnetic head imaging system," *IEEE Transactions on Antennas and Propagation*, vol. 68, pp. 183–194, Jan 2020.

[11] D. O. Rodriguez-Duarte, J. A. Tobon Vasquez, R. Scapaticci, L. Crocco,and F. Vipiana, "Assessing a microwave imaging system for brain stroke monitoring via high fidelity numerical modelling," *IEEE Journal of Electromagnetics, RF and Microwaves in Medicine and Biology*, pp. 1–1, 2021, doi: 10.1109/JERM.2020.3049071, in press.

[12] J. A. Tobon Vasquez et al., "Noninvasive Inline Food Inspection via Microwave Imaging Technology: An Application Example in the Food Industry," in IEEE Antennas and Propagation Magazine, vol. 62, no. 5, pp. 18-32, Oct. 2020, doi: 10.1109/MAP.2020.3012898.

[13] J. LoVetri, M. Asefi, C. Gilmore and I. Jeffrey, "Innovations in Electromagnetic Imaging Technology: The Stored-Grain-Monitoring Case," in IEEE Antennas and Propagation Magazine, vol. 62, no. 5, pp. 33-42, Oct. 2020, doi: 10.1109/MAP.2020.3003206.

[14] M. Bertero and P. Boccacci, Introduction to Inverse Problems in Imaging. Inst. Phys., Bristol, U.K., 1998.

[15] O. Karadima, M. Rahman, J. Sotiriou, N. Ghavami, P. Lu, S. Ahsan, and P. Kosmas, "Experimental validation of microwave tomography with the DBIM-TwIST algorithm for brain stroke detection and classification," *SENSORS*, vol. 20, Feb. 2020.

[16] Z. Amer, C. Gilmore and J. LoVetri, "Finite-element contrast source inversion method for microwave imaging," in Inverse Problems, vol.26, Nov, 2010, doi:10.1088/0266-5611/26/11/115010

[17] G. Giordanengo, M. Righero, F. Vipiana, G. Vecchi and M. Sabbadini, "Fast Antenna Testing With Reduced Near Field Sampling," in IEEE Transactions on Antennas and Propagation, vol. 62, no. 5, pp. 2501-2513, May 2014, doi: 10.1109/TAP.2014.2309338.

[18] E. A. Attardo, A. Borsic, G. Vecchi and P. M. Meaney, "Whole-System Electromagnetic Modeling for Microwave Tomography," in IEEE Antennas and Wireless Propagation Letters, vol. 11, pp. 1618-1621, 2012, doi: 10.1109/LAWP.2013.2237745.

[19] J. A. Tobon Vasquez et al., "A Prototype Microwave System for 3D Brain Stroke Imaging," in Sensors, vol.20, no. 9, May 2020, doi: 10.3390/s20092607

[20] D. O. Rodriguez-Duarte, J. A. Tobon Vasquez, R. Scapaticci, L. Crocco and F. Vipiana, "Brick Shaped Antenna Module for Microwave Brain Imaging Systems," in IEEE Antennas and Wireless Propagation Letters, doi: 10.1109/LAWP.2020.3022161.

[21] G. H. Golub and C. F. Van Loan, Matrix computations, 3rd ed. Baltimore, MD, USA: Johns Hopkins Univ. Press, 1996.

[22] N. Joachimowicz, B. Duchene, C. Conessa, and O. Meyer, "Anthropomorphic breast and head phantoms for microwave imaging," Diagnostics, vol. 85, pp. 1–12, Dec. 2018.